catalysts

MDPI

Article

Photocatalytic Hydrogen Generation from Aqueous Methanol Solution over *n*-Butylamine-Intercalated Layered Titanate $H_2La_2Ti_3O_{10}$: Activity and Stability of the Hybrid Photocatalyst

Ivan A. Rodionov [1,*], Ekaterina O. Gruzdeva [1], Anton S. Mazur [2], Sergei A. Kurnosenko [1], Oleg I. Silyukov [1] and Irina A. Zvereva [1]

[1] Institute of Chemistry, Saint Petersburg State University, 199034 Saint Petersburg, Russia
[2] Magnetic Resonance Research Center, Saint Petersburg State University, 199034 Saint Petersburg, Russia
* Correspondence: i.rodionov@spbu.ru

Abstract: The stability of platinized *n*-butylamine-intercalated layered titanate $H_2La_2Ti_3O_{10}$ during the process of photocatalytic hydrogen production from aqueous methanol under UV irradiation has been thoroughly investigated by means of XRD, CHN, TG, ^{13}C NMR, BET, SEM and GC-MS analysis. It was revealed that *n*-butylamine completely abandons the interlayer space and transforms into *n*-butyraldehyde within 3 h of the reaction, while the particle morphology and specific surface area of the photocatalyst are preserved. The resulting solid phase contains carbon in at least two different oxidation states, which are attributed to the intermediate products of methanol oxidation bound to the perovskite matrix. The activity of the photocatalyst formed in this way is stable in time and strongly depends on the medium pH, which is not typical of either the parent $H_2La_2Ti_3O_{10}$ or TiO_2. An approximate linear equation $\varphi \approx 29–2 \cdot pH$ holds for the apparent quantum efficiency of hydrogen production in the 220–340 nm range at 1 mol. % methanol concentration. In the acidic medium, the photocatalyst under study outperforms the platinized $H_2La_2Ti_3O_{10}$ by more than one order of magnitude. The variation in methanol concentration allowed a maximum quantum efficiency of hydrogen production of 44% at 10 mol. % to be reached.

Keywords: photocatalysis; hydrogen; layered perovskite; titanate; intercalation; amine; hybrid

Citation: Rodionov, I.A.; Gruzdeva, E.O.; Mazur, A.S.; Kurnosenko, S.A.; Silyukov, O.I.; Zvereva, I.A. Photocatalytic Hydrogen Generation from Aqueous Methanol Solution over *n*-Butylamine-Intercalated Layered Titanate $H_2La_2Ti_3O_{10}$: Activity and Stability of the Hybrid Photocatalyst. *Catalysts* **2022**, *12*, 1556. https://doi.org/10.3390/catal12121556

Academic Editor: Jaime Soler

Received: 6 November 2022
Accepted: 30 November 2022
Published: 1 December 2022

1. Introduction

In recent decades, the world has been facing the aggravation of environmental problems such as the greenhouse effect, global warming as well as water, air and soil pollution, which largely originate from the continued use of fossil fuels. The threat of the resulting energy and ecological crisis motivates researchers and engineers to develop and implement novel environmental remediation approaches, waste-free technologies and renewable energy sources, including hydrogen. The latter is considered a promising energy carrier characterized by unprecedented high calorific value and the absence of secondary pollution being typical of traditional fuels [1–3].

One of the most eco-friendly approaches to hydrogen production is water photoelectrolysis, which was first described by Fujishima and Honda [4] and led to the active development of photoelectrochemical cells and powder photocatalysts [5–14]. At the same time, thermodynamic and kinetic limitations of the water splitting reaction still make it difficult to create highly efficient photocatalytic hydrogen generators [15–17] despite significant progress made in this direction in recent years [18–27]. In this regard, along with the aforementioned water splitting technique, another method for hydrogen production is being actively explored—the photocatalytic conversion of plant biomass and primary products of its processing (methanol, other bioalcohols, carbohydrates, etc.) which allows much greater quantum yields to be achieved [28–36].

Along with the «classic» photocatalyst TiO_2 [37–41] as well as various sulfide- [42,43] and nitride-based [44–46] materials, a significant contribution to the development of photocatalytic hydrogen production was made by the study of ion-exchangeable layered oxides adopting the perovskite structure [47]. Promising photocatalytic properties of these oxides originate from their unique 3D crystal lattice formed by perovskite layers, providing the efficient separation of photoexcited charge carriers and chemically active interlayer spaces [48–52]. Layered perovskite-type oxides open up a vast scope for researchers to carry out various modifications via the topochemical reactions of intercalation and ion exchange [38–47] to optimize photocatalytic performance for a wide range of applications. Furthermore, these materials are amenable to ion substitution in the perovskite block [53–58], conjunction with different cocatalysts and photosensitizers [59–68] as well as exfoliation into perovskite nanosheets [69,70], which allows for the creation of new efficient photocatalysts with a wide light absorption region and high specific surface area. In addition, another intriguing feature of ion-exchangeable layered perovskites is the probable involvement of their interlayer space in the photocatalytic reaction, accommodating reactants from the solution as an additional reaction zone [71–73].

After the substitution of interlayer cations with protons, layered perovskite-type oxides may be used to yield hybrid inorganic–organic materials via the intercalation of organic bases [74–76] or the esterification-like grafting of alcohols [77–79] and other hydroxy compounds [80–82]. The inorganic–organic samples obtained in these ways can not only combine practically significant features of the parent substances in one material but also exhibit new properties not being typical of the initial components [83–85]. Although such hybrid materials have a wide range of promising applications, until recently, they were practically not considered as hydrogen evolution photocatalysts due to the potential photodegradation of the organic modifiers [86]. At the same time, there were some reports on the enhanced activity of layered oxides modified by alkoxy groups [87] and polyaniline [88–90] in relation to the light-driven decomposition of organic dyes as model water contaminants. Moreover, our recent studies have revealed that the organically modified layered perovskite-type oxides $HCa_2Nb_3O_{10}$ and $H_2Ln_2Ti_3O_{10}$ (Ln = La, Nd) demonstrate excellent hydrogen evolution activity in aqueous solutions of methanol [91–94], glucose and xylose [95]. The photocatalytic reaction rate exceeded that observed over the unmodified oxides by more than two orders of magnitude and was stable in time. However, our preliminary studies also revealed that some hybrid photocatalysts experience a pronounced contraction of the interlayer space as a result of photocatalytic reaction, which indicates either the escape or destruction of the inserted organic molecules. This conflict between the stable photocatalytic activity and apparent chemical instability of hybrid photocatalysts motivated us to investigate the ongoing processes more carefully. From our perspective, understanding the chemical nature of hybrid photocatalysts under operation conditions and the reasons for their high and stable activity may lead to significant progress in the future design of new highly efficient photocatalytic systems.

The main purpose of the present work was to characterize the changes that occur in the hybrid photocatalyst during the reaction of hydrogen production from aqueous methanol under UV light. As a research object, we chose one of the most active hybrid photocatalysts we have discovered so far: the layered perovskite-type titanate $H_2La_2Ti_3O_{10}$ intercalated by *n*-butylamine and modified with platinum nanoparticles as a cocatalyst [94]. We investigated the structure, composition, particle morphology and surface area of the photocatalyst before and after the photocatalytic reaction and also analyzed the composition of the reaction solution during the photocatalytic process. Furthermore, we studied the dependence of photocatalytic activity on the medium's pH and methanol concentration. Some experiments were additionally performed for the isostructural titanate $H_2Nd_2Ti_3O_{10}$ modified in the same way for comparison.

2. Results and Discussion

2.1. XRD Analysis

The *n*-butylamine-intercalated titanate $H_2La_2Ti_3O_{10}\times BuNH_2$ (further referred to as $HLT_3\times BuNH_2$) was obtained from the initially synthesized $K_2La_2Ti_3O_{10}$ (KLT_3) by protonation yielding $H_2La_2Ti_3O_{10}$ (HLT_3) followed by subsequent methylamine and *n*-butylamine introduction. According to powder XRD analysis, all the samples were obtained as single-phase products without notable impurities. The XRD patterns and lattice parameters for this series are presented in Figure 1. Corresponding data for the analogous neodymium-containing series $K_2Nd_2Ti_3O_{10}$ (KNT_3), $H_2Nd_2Ti_3O_{10}$ (HNT_3), $H_2Nd_2Ti_3O_{10}\times BuNH_2$ ($HNT_3\times BuNH_2$) have already been reported in [91] and therefore are not presented here.

The most important information provided by XRD in the current study is the degree of expansion or contraction of the space between adjacent perovskite layers during chemical transformations. Due to the possible change in space groups during these transformations, it is convenient to keep track of the interlayer distance *d*, which is the distance between centers of two adjacent perovskite layers and is easily derived from the corresponding unit cell parameter for each space group. These interlayer distances *d* are presented in Table 1.

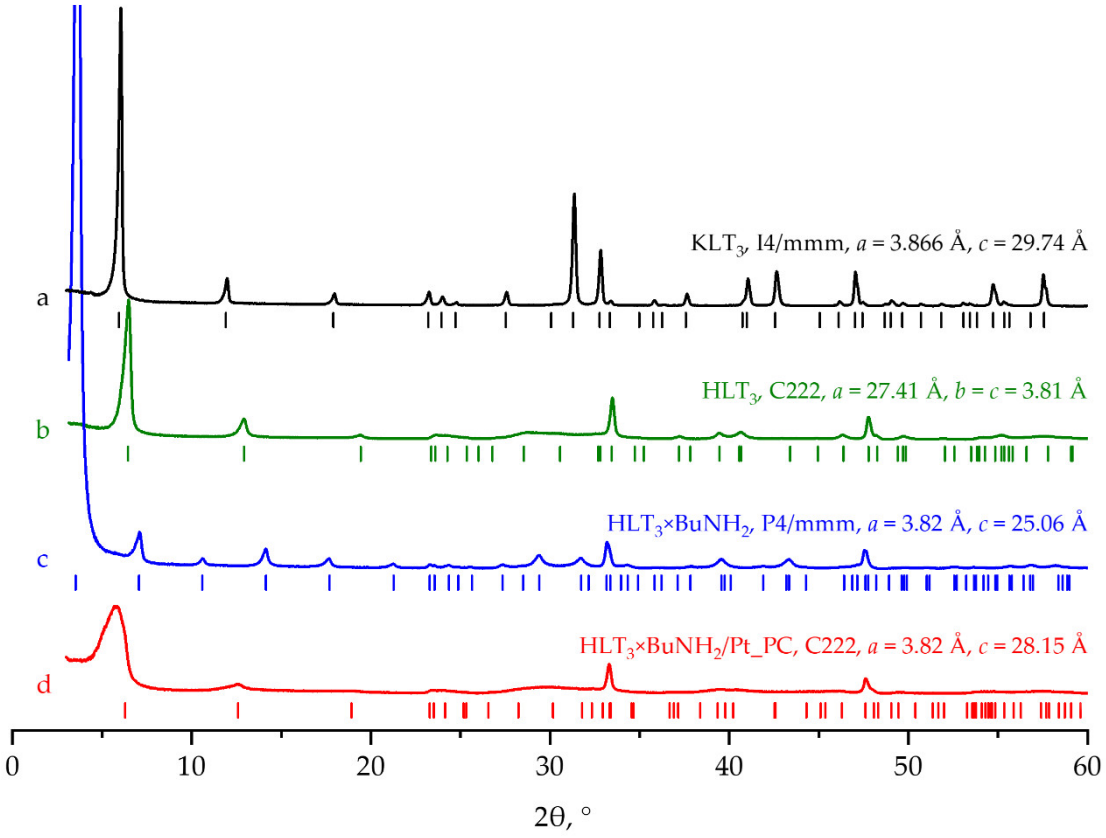

Figure 1. Powder XRD patterns of (**a**) the initial titanate $K_2La_2Ti_3O_{10}$ (KLT_3), (**b**) its protonated form $H_2La_2Ti_3O_{10}$ (HLT_3), (**c**) *n*-butylamine-intercalated form $H_2La_2Ti_3O_{10}\times BuNH_2$ ($HLT_3\times BuNH_2$) and (**d**) platinized *n*-butylamine-intercalated form $H_2La_2Ti_3O_{10}\times BuNH_2$/Pt after 2.5 h of photocatalytic experiment ($HLT_3\times BuNH_2$/Pt_PC).

The initial alkaline form of the layered titanate KLT_3 was indexed in the I4/mmm space group (staggered conformation of perovskite layers) with the lattice parameters slightly enlarged compared to the KNT_3 analog, which is in good agreement with the literature data [96]. After protonation, the interlayer distance *d* decreased from 14.87 Å to 13.71 Å due to the substitution of potassium cations by smaller protons. The subsequent intercalation of *n*-butylamine led to a huge expansion of the interlayer space by 11.35 Å

and to a transition into the P4/mmm space group corresponding to the eclipsed conformation of adjacent perovskite layers.

To prepare the sample "after photocatalysis", 100 mg of HLT_3×$BuNH_2$ was dispersed in 50 mL of 1 mol. % aqueous methanol containing 5.1 μmol H_2PtCl_6 as a platinization agent and irradiated by UV light in the photocatalytic reactor for 150 min—a typical duration of our photocatalytic experiment. The solid sample obtained in this way after centrifugation and drying is further denoted as HLT_3×$BuNH_2$/Pt_PC.

XRD analysis of the HLT_3×$BuNH_2$/Pt_PC sample revealed that the interlayer distance shrunk almost to its original value before butylamine intercalation (HLT_3). This clearly suggests that at least a major part of the intercalated butylamine left the interlayer space via either deintercalation or photocatalytic degradation. Furthermore, the XRD pattern of HLT_3×$BuNH_2$/Pt_PC compared to HLT_3 showed strong anisotropy—particularly, the low-angle peaks, whose positions depend exclusively on the interlayer distance *d*, were significantly broadened. This may be explained by the stacking disorder of perovskite layers that arises from intensive reactions taking place in the interlayer space, accompanied by the escape of butylamine molecules. In the case of the neodymium-containing analog HNT_3×$BuNH_2$/Pt_PC, this effect of the anisotropic broadening was much more pronounced and, thus, did not allow us to estimate the interlayer distance even approximately.

Table 1. The content of carbon and nitrogen per formula unit of the layered oxide determined by CHN analysis and the interlayer distance *d* for the samples of protonated (HLT_3 and HNT_3), methylamine-intercalated (HLT_3×$MeNH_2$ and HNT_3×$MeNH_2$) and *n*-butylamine-intercalated (HLT_3×$BuNH_2$ and HNT_3×$BuNH_2$) layered titanates, and the platinized samples after photocatalytic experiments (HLT_3×$BuNH_2$/Pt_PC and HNT_3×$BuNH_2$/Pt_PC).

Sample	C	N	*d*, Å
HLT_3	0	0	13.71
HNT_3	0	0	13.59 [1]
HLT_3×$MeNH_2$	0.9	1.1	21.94
HNT_3×$MeNH_2$	1.0	1.2	21.98 [1]
HLT_3×$BuNH_2$	4.3	0.9	25.06
HNT_3×$BuNH_2$	4.2	0.9	24.70 [1]
HLT_3×$BuNH_2$/Pt_PC	1.0	0	≈14.1
HNT_3×$BuNH_2$/Pt_PC	0.9	0	–

[1] Data from our previous work [91].

2.2. CHN Analysis

The results of elemental CHN analysis shown in Table 1 support the XRD data quite well. As can be seen, the determined amounts of carbon and nitrogen per formula unit of the layered oxide were in good agreement with the expected values corresponding to one molecule of methylamine and *n*-butylamine per formula unit. Having said so, both lanthanum- and neodymium-containing samples included similar amounts of the interlayer amine molecules. However, after the photocatalytic reaction, we did not detect nitrogen in either of the samples, while the carbon content decreased by 4 times. The chemical nature of the remaining carbon is not clear yet, but its presence explains the slightly enlarged interlayer distance compared to that of the initial protonated form.

2.3. TG Analysis

The above results are supplemented by thermogravimetric analysis data (Figure 2). The TG curve of the protonated sample HLT_3, as usual, demonstrates two steps of mass loss: the first one (T < 200 °C) caused by the deintercalation of small amounts of water and the second one (280 °C < T < 600 °C) corresponding to the complete thermolysis of the layered oxide $H_xK_{2-x}La_2Ti_3O_{10}$ with the liberation of water to form residual

$K_{2-x}La_2Ti_3O_{10-x/2}$. Based on the mass losses at these two steps, we calculated the protonation degree ($x/2 = 0.83$) and the amount of intercalated water per formula unit ($y = 0.22$) according the procedure described in [97].

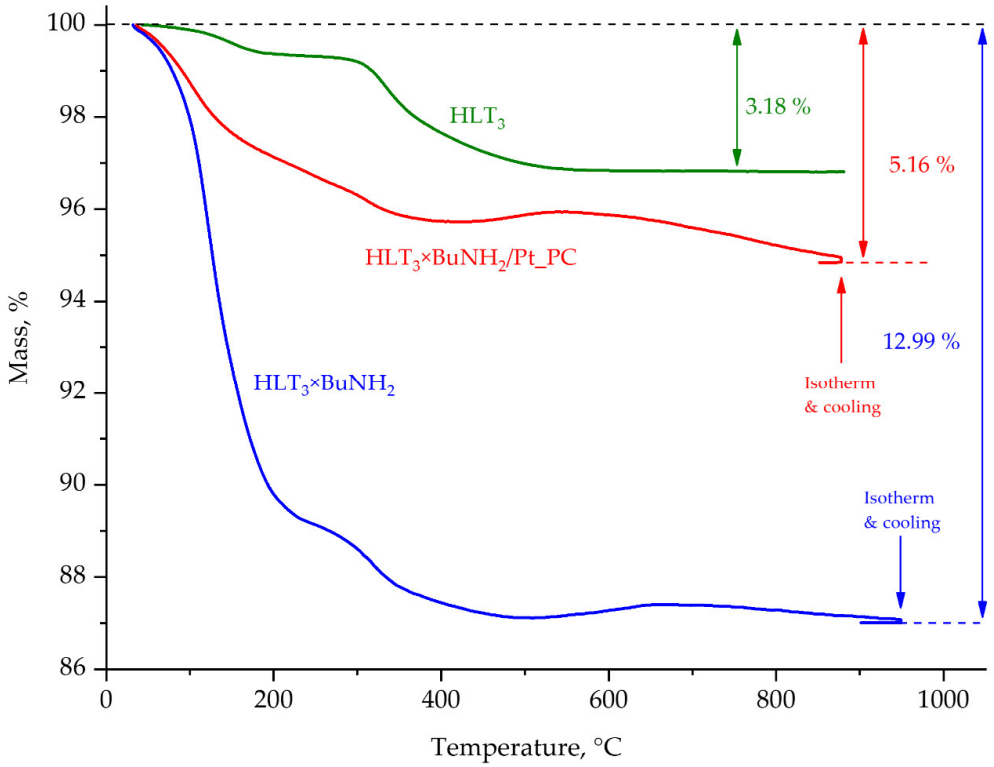

Figure 2. Thermogravimetric curves for the protonated titanate (HLT_3), its *n*-butylamine-intercalated form (HLT_3×$BuNH_2$) and the platinized *n*-butylamine-intercalated form after photocatalytic experiment (HLT_3×$BuNH_2$/Pt_PC).

The TG curve of HLT_3×$BuNH_2$ shows a total mass loss as high as 12.99%, which is not separated so easily into distinct consecutive steps. If we subtract the mass loss of 2.27%, which has to be due to the thermolysis of the protonated form, and assume the residual 10.72% to correspond solely to the butylamine (although there might also be some minor amount of water and/or methylamine), we obtain 0.99 butylamine molecules per formula unit, which is consistent with the CHN analysis data. The increase in mass observed between 450 °C and 650 °C is typical of such types of hybrid materials [94] and is caused by the partial oxidation of organic molecules, which do not liberate at low temperatures but remain bound to the perovskite matrix. At sufficiently high temperatures, the oxidation of such species finally leads to gaseous CO_2 and, thus, the mass of the sample falls again.

The TG curve of the sample after the photocatalytic reaction (HLT_3×$BuNH_2$/Pt_PC) clearly indicates that at least a major part of *n*-butylamine left the interlayer space. On the other hand, we see that this sample is by no means identical to the initial protonated form HLT_3. We still observe the stage of mass increase, which is typical of oxidizable organic-containing samples, although this stage shifted to lower temperatures by ca. 80 °C compared to HLT_3×$BuNH_2$. In addition, the total mass loss was almost 2% greater compared to HLT_3. Unfortunately, we cannot draw any further quantitative conclusions from these results without knowledge of the specific nature of residual organic species in the sample. By now, we can only state that during the photocatalytic reaction, the butylamine-intercalated sample HLT_3×$BuNH_2$ did not return to the original protonated form HLT_3 or some of its hydrated derivatives—it still contained certain amounts of organics capable of oxidation in the air atmosphere at elevated temperature.

2.4. ^{13}C NMR Analysis

The disappearance of butylamine from the interlayer space during the photocatalytic reaction was also confirmed via solid-state ^{13}C NMR spectroscopy. As can be seen from Figure 3, before the irradiation of the $HLT_3 \times BuNH_2$ sample, four distinct peaks were clearly detected, corresponding to the four carbon atoms in the $BuNH_3^+$ cation. Note that this first sample was not just the original $HLT_3 \times BuNH_2$ but it was the one dispersed in the 1 mol. % methanol solution containing H_2PtCl_6 and subjected to ultrasonic treatment in exactly the same way as during the other photocatalytic experiments. The only difference is that the sample was separated from the solution and dried without being irradiated, unlike the other samples in this series. Upon the irradiation, the four peaks of *n*-butylamine gradually decreased, and after 150 min, only a low-intensity broad peak remained in the corresponding region of a chemical shift. Additionally, a new low-field shifted peak appeared in the region of 175 ppm which can typically be attributed to carboxylic acid derivatives.

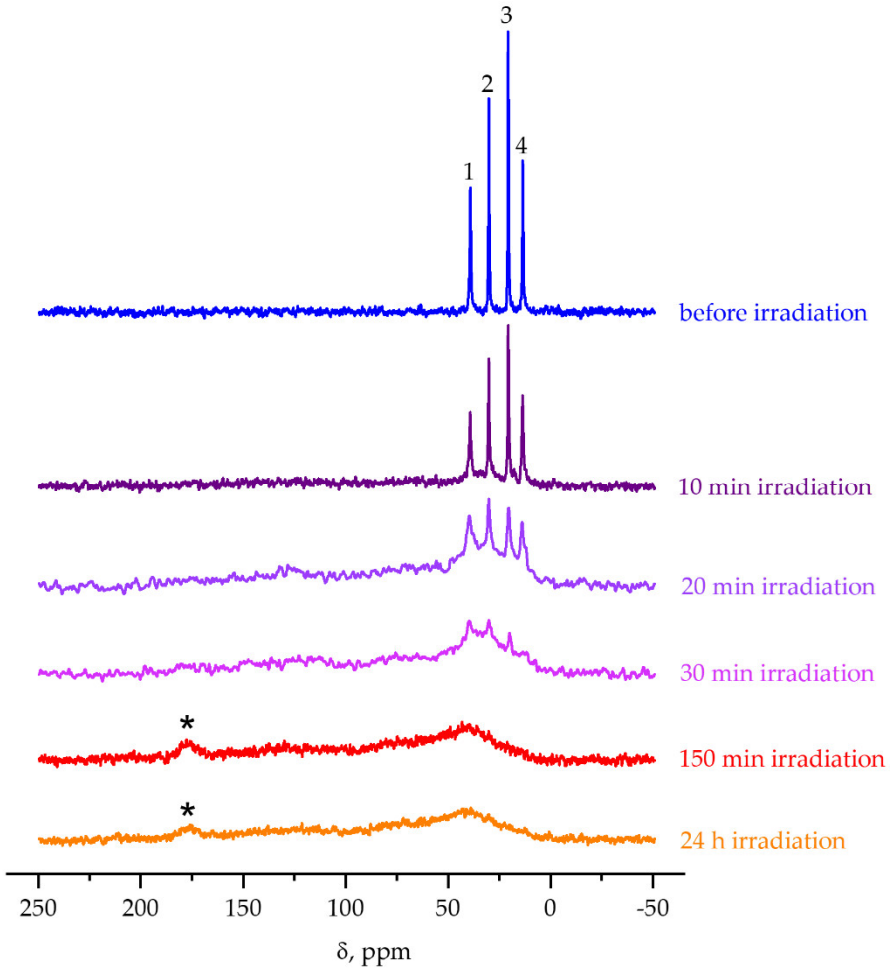

Figure 3. ^{13}C solid-state NMR spectra of the *n*-butylamine-intercalated titanate $HLT_3 \times BuNH_2$ after different times of irradiation in 1 mol. % aqueous methanol solution with H_2PtCl_6 additive (standard photocatalytic conditions); 1, 2, 3, 4–characteristic peaks of *n*-butylammonium, *—new peak corresponding to carbon in oxidized state.

Although the NMR spectra obtained are not as informative as one would like, we can conclude that the carbon, which was contained in the $HLT_3 \times BuNH_2$/Pt_PC sample in an approximate amount of one atom per formula unit, was present at least in two different oxidation states with chemical shifts around 40 and 175 ppm. We have to emphasize that this remaining carbon was likely to originate not from the intercalated *n*-butylamine but

rather from the methanol in the reaction solution. During the photocatalytic process, compact methanol molecules may easily penetrate into the interlayer space, especially as long as it remains expanded by the intercalated *n*-butylamine. Once inserted, methanol molecules can readily undergo photocatalytic oxidation, forming a whole cocktail of intermediate products, which may be bound to the perovskite matrix in different ways. Taking into account the relatively low total mass loss of the $HLT_3{\times}BuNH_2$/Pt_PC sample (5.16%) together with the estimated content of one carbon per formula unit, one can conclude that the main part of the organic species must be bound to the inorganic matrix rather than represent individual intercalated molecules. According to known data on photocatalytic methanol oxidation over TiO_2 and other oxides [98–100], these might be interlayer methoxy groups (Ti-OCH_3), chemically bound formaldehyde (Ti-OCH_2), formyl (Ti–OCH) and formate ((Ti-$O)_2CH^-$) groups. It is important to note the NMR spectrum hardly changed in its appearance even after 24 h of the photocatalytic reaction, suggesting that a quasi-stationary state was established, which is consistent with the fact of its stable photocatalytic performance.

2.5. BET and SEM

Measurements of the BET specific surface area revealed that the initial *n*-butylamine-intercalated sample ($HLT_3{\times}BuNH_2$) and the sample after photocatalytic experiment ($HLT_3{\times}BuNH_2$/Pt_PC) had almost the same specific area of 15.3 m^2/g and 12.7 m^2/g, respectively. This indicates that no considerable delamination of the layered structure occurred during the photocatalytic process, which could otherwise have strongly affected the photocatalytic activity of the sample. SEM investigations also confirmed that the initial plate-like particle morphology of $HLT_3{\times}BuNH_2$ was preserved after the photocatalytic experiment (Figure 4). This is in agreement with our previous reports on analogous hybrid photocatalysts [91,94]. The deposited platinum nanoparticles can be seen on the SEM image as light dots distributed over the surface of $HLT_3{\times}BuNH_2$/Pt_PC particles.

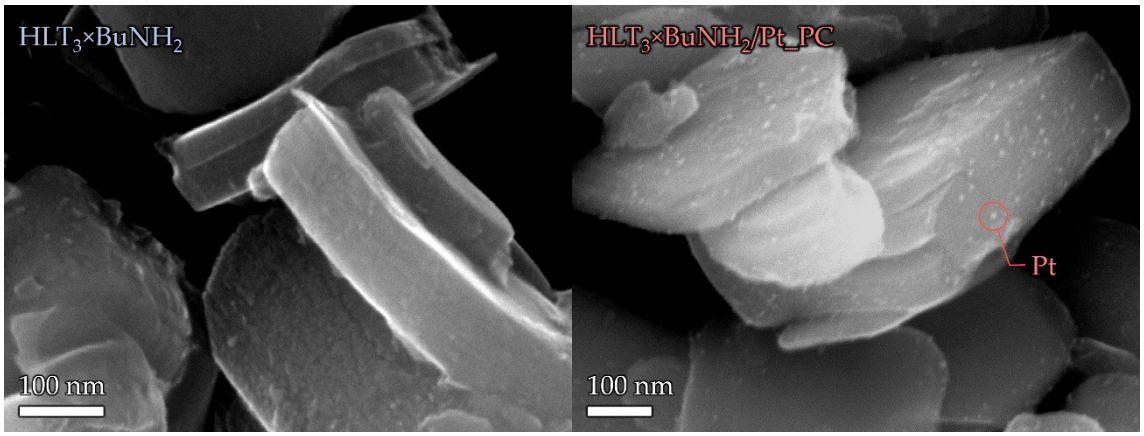

Figure 4. SEM images of the *n*-butylamine-intercalated titanate before ($HLT_3{\times}BuNH_2$) and after ($HLT_3{\times}BuNH_2$/Pt_PC) the photocatalytic experiment.

2.6. GS-MS Analysis of Solution

As a final approach to investigate the processes occurring during the irradiation of $HLT_3{\times}BuNH_2$ in the methanol solution, we analyzed the liquid phase in the course of the photocatalytic experiment by means of GC-MS. For this, we carried out a long-term 12 h experiment sampling 1 mL of the reacting suspension for analysis every 1 h. Between sampling, the rate of hydrogen evolution was also measured. Unfortunately, we did not get the opportunity to make a reliable quantitative calibration of the GC-MS for the detected components, so the results presented only reflect the relative changes in concentration, but not their absolute values.

As can be seen from Figure 5, at the starting point prior to irradiation, the solution already contained a certain amount of *n*-butylamine, which deintercalated from $HLT_3 \times BuNH_2$ during the preparation of the suspension. In the course of the next 3 h, the butylamine concentration gradually decreased to almost zero, while a new component, *n*-butyraldehyde, was rapidly produced, reaching its peak concentration after around 2 h. It is natural to assume that the butyraldehyde is formed from the butylamine by photocatalytic oxidation and is an intermediate product since its concentration gradually decreased throughout the experiment after 2 h. Despite the undoubted complexity of ongoing processes, the kinetic curves of both butylamine and butyraldehyde are surprisingly good, described by the standard kinetic model of consecutive first-order reactions A → B (k_1); B → C (k_2) with apparent rate constants $k_1 = 1.41\ h^{-1}$, $k_2 = 0.20\ h^{-1}$.

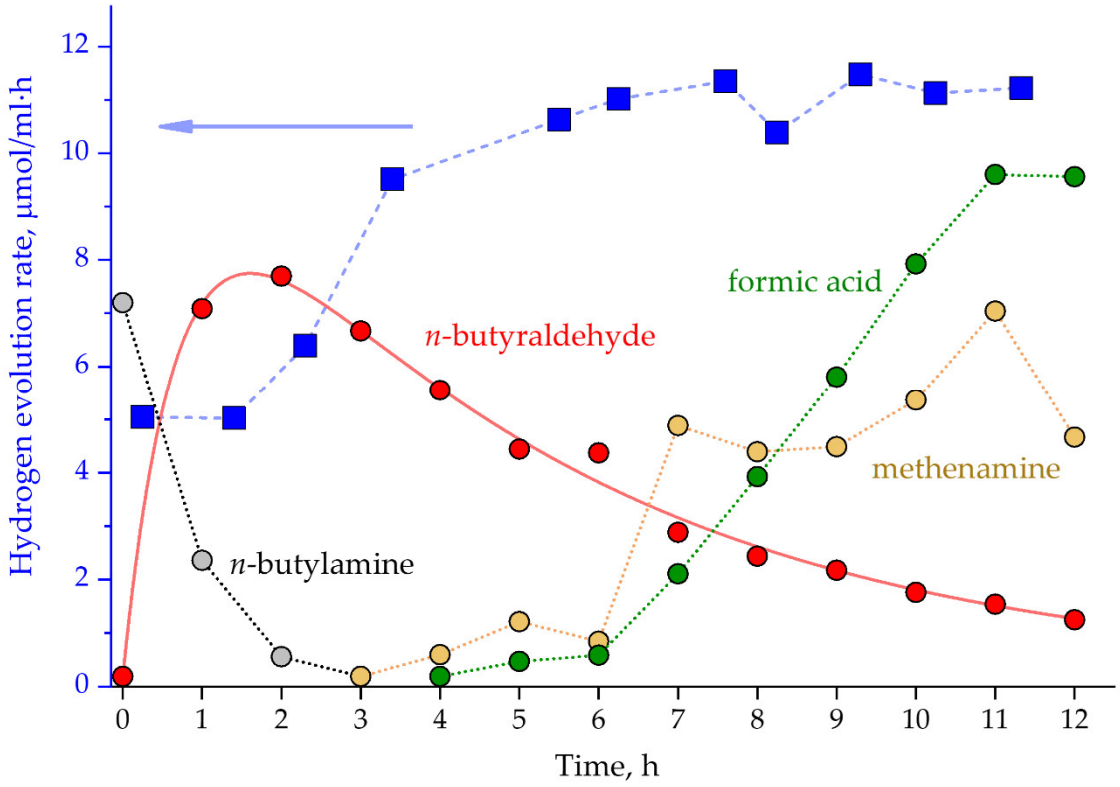

Figure 5. Dynamics of the main components detected via GC-MS in the reaction solution during photocatalytic hydrogen evolution over $HLT_3 \times BuNH_2$/Pt from 1 mol. % aqueous methanol for 12 h and the change in hydrogen evolution rate.

Attention should be paid to the time interval around 3 h—by this time, the butylamine was almost completely consumed, and simultaneously, we observed a sharp increase in the hydrogen generation rate. It was also not until this time that we started detecting two other main products—formic acid and methenamine. Formic acid is a natural oxidation product of methanol, while methenamine is probably formed by the condensation of formaldehyde and ammonia, and the latter is released from butylamine during its conversion to butyraldehyde. The above reactions are schematically presented in Figure 6.

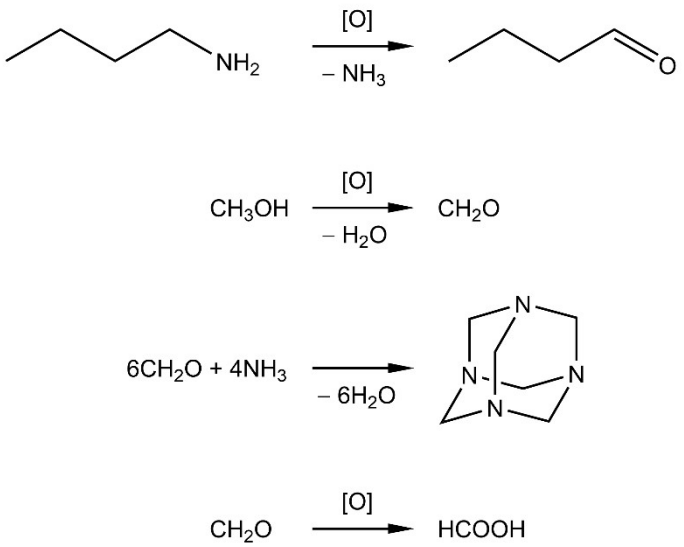

Figure 6. Supposed scheme of formation of the main products detected in the reaction solution during photocatalytic hydrogen evolution over HLT_3×$BuNH_2$/Pt from 1 mol. % aqueous methanol.

One possible reason why 3 h is such a critical point at the reaction timeline regarding the hydrogen evolution rate may be the change in the solution pH. By the start of the reaction, the measured pH value was 10.2, which was due to the basic nature of *n*-butylamine. By the end of the experiment, however, the pH value already dropped below 3.5. This is easily explained because basic butylamine is decomposed and acidic species are also formed during methanol oxidation. Thus, it should have been right between 2 and 4 h that the pH value changed most significantly, although we did not monitor it during this experiment. The effect of the acceleration of hydrogen evolution with time found during this long-term experiment was quite surprising to us, because typically, we limited the experiment time by 2.5 h, which was clearly insufficient for this effect to occur.

Concerning the stability of photocatalytic performance, the hydrogen evolution rate stayed almost constant from 5 to 12 h of the experiment time. The total amount of hydrogen evolved during this experiment from every 1 mL of the reaction mixture was approximately 110 μmol, while the photocatalyst content in every 1 mL was only 3 μmol. The 36-fold excess of the formed product relative to the catalyst indicates the process under study to be truly photocatalytic, without the significant consumption or deactivation of the solid photocatalyst.

To conclude the discussion of this experiment, we should mention that other products, besides the ones presented in Figure 5, including formaldehyde, formamide, butyramide and *n*-butylformamide, were also detected in the reaction medium in minor amounts. They were mostly accumulated during the first two hours of the experiment and did not show considerable concentration dynamics throughout the further experiment.

2.7. Effect of pH on the Photocatalytic Activity

In order to confirm our hypothesis concerning the reaction acceleration, we decided to examine the effect of pH on the hydrogen evolution rate separately. For this aim, we employed our standard experimental conditions (photocatalyst concentration 0.5 g/L in 1 mol. % methanol, 1 wt. % platinum loading) and adjusted the pH value by the addition of HCl or KOH directly to the reaction mixture after platinum had been deposited under identical initial conditions. In addition to HLT_3×$BuNH_2$, we also chose the protonated sample without butylamine (HLT_3) and TiO_2 P25 Evonic-Degussa as photocatalysts for comparison.

The results presented in Figure 7 show that the acidic medium indeed favors the photocatalytic performance of HLT_3×$BuNH_2$/Pt: the difference in apparent quantum

efficiency at pH < 3 and pH > 12 was about one order of magnitude. This is in contrast with the data obtained for both HLT_3/Pt and TiO_2/Pt. The photocatalytic activity of the platinized layered oxide HLT_3 without intercalated butylamine was overall quite poor and hardly exceeded 1% on the quantum efficiency scale, being almost the same at natural pH = 4.6 and basic pH = 11.15 and dropping even lower at pH = 3 (φ = 0.6%). As expected, platinized titania showed much better performance; however, at pH values below 4, its efficiency also decreased. This behavior is consistent with the literature data [101] and is explained by the protonation ($-OH_2^+$) and dissociation ($-O^-$) of OH-groups on the surface of TiO_2 in acidic and basic medium, respectively, which affects the adsorption properties of both the surface and the particle agglomeration. As a result, the optimal pH for the photocatalytic reaction lies around the neutral region, and the overall effect of pH on the reaction rate is not crucial (the observed difference at extreme points may be around 2.5 times). As we see, the same tendency also approximately held for HLT_3. However, the amine-intercalated sample HLT_3×$BuNH_2$/Pt strongly deviated from its «classic» analogs, showing an abnormally high pH dependence of photocatalytic activity. The reason for such behavior is unclear. Hopefully, future studies will explain this phenomenon based on the chemical and structural nature of the catalyst, which has not been completely determined yet, despite our efforts.

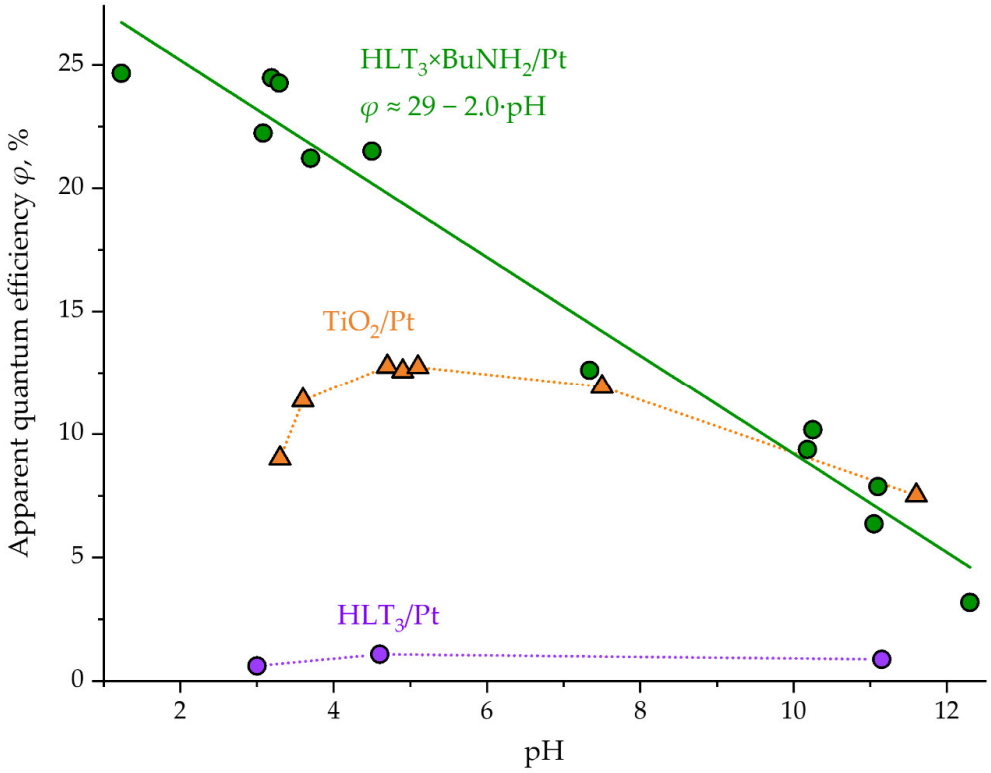

Figure 7. Dependence of apparent quantum efficiency of hydrogen evolution from 1 mol. % aqueous methanol on the solution pH for the platinized titanate HLT_3/Pt, its *n*-butylamine-intercalated form HLT_3×$BuNH_2$/Pt and platinized TiO_2 P25 for comparison.

2.8. Effect of Methanol Concentration on the Photocatalytic Activity

As a final point in this work, we investigated the dependence of the hydrogen evolution rate on the methanol concentration. We already reported this dependence for HNT_3×$BuNH_2$/Pt in the concentration range of 0–10 mol. % [91]. Then, we extended the concentration range up to 30 mol. % and supplemented the study with data for HLT_3×$BuNH_2$/Pt and platinized TiO_2 P25 for comparison (Figure 8).

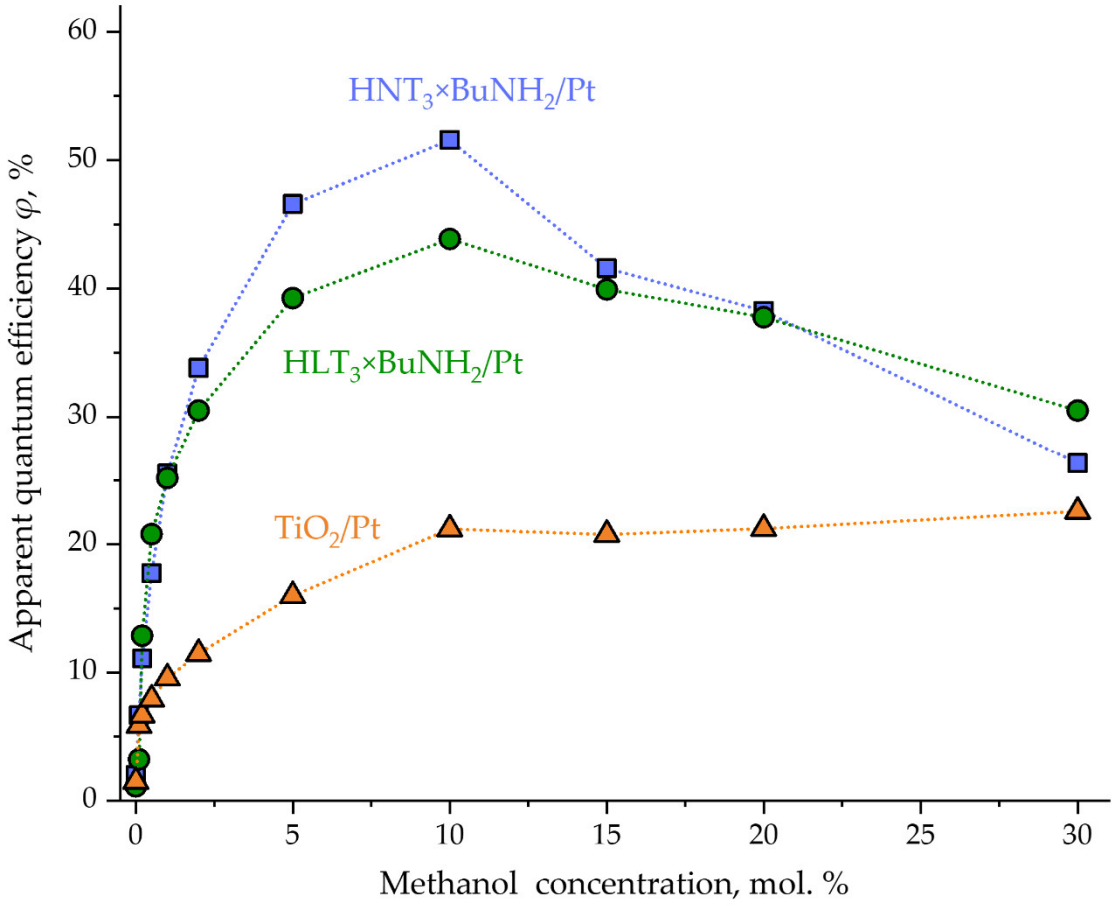

Figure 8. Dependence of apparent quantum efficiency of hydrogen evolution on the methanol concentration for the platinized *n*-butylamine-intercalated titanates HLT3×BuNH2/Pt, HNT3×BuNH2/Pt and platinized TiO_2 P25 for comparison.

Platinized titania behaves quite naturally—the reaction rate increases rapidly at a low methanol concentration and reaches saturation at 10 mol. % with an apparent quantum efficiency around 20%. This is consistent with the usually adopted Langmuir–Hinshelwood model for heterogeneous catalysis. Both HLT3×BuNH2/Pt and HNT3×BuNH2/Pt samples show overall similar behavior at low methanol concentrations with the only difference being their greater activity. However, after the maximum quantum efficiency is reached at 10 mol. % ($\varphi \approx 44\%$ for HLT3×BuNH2/Pt and $\varphi \approx 52\%$ for HNT3×BuNH2/Pt), both curves start to decrease, and this effect is more pronounced for the more active HNT3×BuNH2/Pt than for HNT3×BuNH2/Pt. This is another case where an unusual kinetic dependence is observed for hybrid samples under investigation.

We propose two possible reasons for such behavior. Firstly, it may reflect the fact that both methanol and water are involved in the reaction mechanism and, thus, they both should be present in considerable concentrations for the reaction to proceed efficiently. We have already reported [92–94] that the photocatalytic activity of hybrid photocatalysts correlates with the degree of their interlayer hydration, and the same trend also holds for layered oxides without organic modifiers [96,102,103]. This highlights the important role of intercalated water molecules in the mechanism of hydrogen production, and, thus, if the availability of water molecules for the interlayer space decreases, one can also expect some drop in the reaction rate. Secondly, we should emphasize that during these measurements, platinum was deposited on the samples in situ, i.e., in each experiment, during deposition, the concentration of methanol was different. The methanol concentration can potentially affect the properties of deposited platinum nanoparticles in terms of their size, surface distribution, etc., which may, in turn, lead to a change in photocatalytic activity.

This effect did not reveal itself in the case of TiO_2, but it certainly could be felt in the case of more complex organically modified layered oxides HLT_3×$BuNH_2$ and HNT_3×$BuNH_2$. Overall, based on the results obtained, we believe that the process of platinum deposition can play a crucial role in the formation of active photocatalysts from organically modified layered oxides. Particularly, the presence of intercalated organic molecules opens up the potential possibility of platinum deposition not only on the outer surface of the photocatalyst particles but also between the perovskite layers. This process deserves special investigation and is the subject of our current studies.

2.9. Applications of Obtained Results

As for practical applications of the results obtained in this study, we would like to mention the following:

- We clearly demonstrated that the inorganic–organic hybrid material HLT_3×$BuNH_2$ is unstable under the photocatalytic reaction conditions. This fact should be strictly considered in future works devoted to photocatalytic properties of related compounds in order to give a correct interpretation of observed phenomena. At first glance, the high and stable photocatalytic performance may give the misleading impression that the catalyst itself is also chemically stable. However, as we see, this is not necessarily the case. Possible transformations of the photocatalyst during the reaction should always be examined carefully.
- Despite the observed instability of the inorganic–organic hybrid under the photocatalytic reaction conditions, we still claim that the organic modification of layered oxides is a promising strategy to create highly efficient photocatalytic systems. The reason for that is again the stable photocatalytic activity of the material formed during photocatalysis, which is many times higher than that of the initial unmodified sample. Why there is such a pronounced difference is not yet clear, but hopefully, it will be explained in future studies.
- The transformation of *n*-butylamine into *n*-butyraldehyde observed during the photocatalytic reaction led us to the idea that such systems could have a potential synthetic application. Principally, there is nothing new in applying photocatalysis for organic synthesis. However, the fact that the reactant molecules are intercalated into the interlayer space of the photocatalyst may strongly affect the efficiency and selectivity of the ongoing reaction as compared to the usual case when the reaction takes place on the surface of a bulk photocatalyst. Special studies are needed to test this hypothesis.

3. Materials and Methods

3.1. Synthesis of the n-Butylamine-Intercalated Titanates

The synthesis procedure of the layered oxides under study has already been reported in detail in our previous works [91,94], so here, we will describe it only briefly. The initial alkaline forms of layered titanates $K_2La_2Ti_3O_{10}$ (KLT_3) and $K_2Nd_2Ti_3O_{10}$ (KNT_3) were obtained via the solid-state synthesis from K_2CO_3, TiO_2 and La_2O_3 (or Nd_2O_3) as starting reagents (Vekton, Saint Petersburg, Russia, 99.9%). Stoichiometric amounts of TiO_2 and La_2O_3 (or Nd_2O_3) were mixed together with a 50% excess of K_2CO_3, ground under an *n*-heptane layer in a planetary micro mill with a silicon nitride bowl, dried, pressed into pallets and calcined at 1000 °C for 10 h in corundum crucibles.

The protonated forms $H_2La_2Ti_3O_{10}$ (HLT_3) and $H_2Nd_2Ti_3O_{10}$ (HNT_3) were obtained from the corresponding alkaline forms via the ion exchange reaction with an excess of 0.1 M hydrochloric acid for 7 days under continuous stirring at room temperature. Before the reaction, KLT_3 and KNT_3 were exposed to humid air (RH = 75%) overnight to achieve preliminary water intercalation. The solids obtained were separated from the solution via centrifugation at 3000 RCF and dried over CaO.

The intercalation of *n*-butylamine ($BuNH_2$) into the protonated forms was conducted in two steps with the intermediate intercalation of methylamine ($MeNH_2$). In the first step, 12 g of HLT_3 (or HNT_3) was dispersed in 120 mL of the 38% aqueous $MeNH_2$ solution and stirred in a closed flask at 60 °C for 10 d. In the second step, the separated and dried solid denoted as $HLT_3{\times}MeNH_2$ (or $HNT_3{\times}MeNH_2$) was dispersed in 80 mL of *n*-butylamine together with 10 mL of water, stirred in a closed flask at room temperature for 4 d, separated and dried. The solid samples obtained, denoted as $HLT_3{\times}BuNH_2$ and $HNT_3{\times}BuNH_2$, were further used for photocatalytic experiments as the main objects of investigation in this work.

3.2. Characterization of Hybrid Photocatalysts

Powder X-ray diffraction (XRD) analysis was performed in each step of synthesis on a Rigaku Miniflex II diffractometer (Tokyo, Japan) using CuKα radiation, 2θ range of 3–60° and a scan speed of 10°/min. The XRD patterns obtained were indexed, and the unit cell parameters were determined using DiffracPlus Topas 4.2 software provided by Bruker (Billerica, MA, USA).

The amounts of carbon, hydrogen and nitrogen in the inorganic–organic hybrids were determined via elemental CHN analysis on a Euro EA3028-HT analyzer (Pavia, Italy).

Thermogravimetric (TG) analysis was carried out on a Netzsch TG 209 F1 Libra microbalance (Selb, Germany) in synthetic dry air atmosphere. The temperature program included heating of the samples from room temperature to 880–950 °C at a rate of 10 °C/min followed by a 20 min isotherm stage.

Solid-state nuclear magnetic resonance spectra (^{13}C NMR) were recorded on a Bruker Avance III 400 WB spectrometer (Billerica, MA, USA) at an operating frequency of 100.64 MHz using a CP/MAS technique. Tetramethylsilane was used as an external reference.

The specific surface area of the samples was determined by the Brunauer–Emmett–Teller (BET) method on a Quadrasorb SI analyzer (Boynton Beach, FL, USA) using nitrogen as an adsorptive gas.

The morphology of the samples was investigated via scanning electron microscopy (SEM) on the Zeiss Merlin scanning electron microscope with a field emission cathode, electron optics column GEMINI-II and oil-free vacuum system.

The liquid-phase products of the photocatalytic reaction were identified on a gas chromatograph–mass spectrometer Shimadzu GCMS-QP2010 Ultra (Kyoto, Japan) equipped with an AOC-5000 Plus autosampler and a Rxi-624Sil MS column (30 m, 0.25 mm, 1.4 μm). The separation was conducted using a program of a temperature increase from 40 °C to 280 °C for 10 min. Helium was used as a carrier gas.

3.3. Photocatalytic Experiments

Photocatalytic experiments were carried out on a self-made laboratory setup, which had been employed in our previous works [91–94]. A certain mass of a photocatalyst sample (typically 30 mg) was dispersed in 60 mL of the aqueous methanol solution of the desired concentration, by default, 1 mol. %. After ultrasonic treatment for 10 min in an Elmasonic S10H bath (Singen, Germany), 50 mL of the photocatalyst suspension was introduced into the external-irradiation reaction cell equipped with quartz windows, a magnetic stirrer, a thermostatic liquid cut-off filter (aqueous solution of KCl and NaBr, 6 g/L each, 2 cm optical path, cut-off wavelength λ < 220 nm, T = 20 °C) and connected to a closed gas circulation system (120 mL constant volume). To achieve in situ platinization of the photocatalyst samples, 1 mL of the 1.27 mM H_2PtCl_6 aqueous solution was also added to the reaction suspension, which corresponded to a platinum content of 1 wt. % in the final composite photocatalyst. Before the start of the photocatalytic reaction, argon was purged through the suspension and gas circulation system for 20 min to remove and substitute the residual air. During the experiment, the photocatalyst suspension was irradiated using a 125 W medium-pressure mercury lamp (DRT-125), and the amount of

hydrogen accumulated in the circulating gas mixture was determined every 5 min via a gas chromatograph Shimadzu GC-2014 (Kyoto, Japan) equipped with an Rt-Msieve 5A column and a TCD, using Ar as a carrier gas. When necessary, the system was intermediately purged with argon for 15 min to blow away the accumulated hydrogen and normalize the increased pressure. As a result, kinetic curves of hydrogen evolution were obtained, and the rate of the photocatalytic reaction was calculated from the slope of these curves. The apparent quantum efficiency φ was calculated by dividing the rate of hydrogen evolution by twice the incident photon flux with energy greater than the photocatalyst bandgap. The photon flux was determined via the advanced ferrioxalate actinometry method, as described in detail in [91].

When the effect of solution pH on the photocatalytic activity was investigated, the pH value was adjusted by the addition of small amounts of HCl or KOH directly to the reaction medium after the platinum deposition had been completed. The pH value was controlled using a Mettler Toledo SevenCompact S220 pH-meter (Greifensee, Switzerland) equipped with an InLab Expert Pro-ISM electrode.

The aim of some photocatalytic experiments was not only to measure the hydrogen evolution rate but also to prepare the samples of photocatalysts after the reaction for further analysis. In the case of such preparative experiments, the initial amount of the photocatalyst was increased 4-fold (120 mg per 60 mL of solution), and so was the concentration of H_2PtCl_6 to preserve the same platinum content in the sample (1 wt. %). The photocatalyst after the reaction was separated from the solution via centrifugation at 3000 RCF and dried over CaO for 24 h. The samples obtained from $HLT_3{\times}BuNH_2$ and $HNT_3{\times}BuNH_2$ in the described manner after 150 min of the photocatalytic reaction are denoted as $HLT_3{\times}BuNH_2$/Pt_PC and $HNT_3{\times}BuNH_2$/Pt_PC. The same conditions were also applied to the long-term photocatalytic experiment when the reaction solution was analyzed.

4. Conclusions

It was established that the platinized *n*-butylamine-intercalated layered titanate $H_2La_2Ti_3O_{10}{\times}BuNH_2$/Pt, which had previously been reported as a highly efficient photocatalyst for hydrogen production from aqueous methanol under UV irradiation, is unstable under operating conditions. Specifically, the intercalated butylamine molecules abandon the interlayer space and are oxidized to butyraldehyde, which undergoes further transformation. Despite this, the remaining solid phase demonstrates unprecedented high and stable photocatalytic activity with respect to hydrogen evolution compared to the initial protonated titanate $H_2La_2Ti_3O_{10}$. The characterization of the solid phase formed after photocatalysis revealed that it contains significant amounts of carbon in at least two different oxidation states, which can be attributed to the intermediate products of methanol oxidation bound to the perovskite matrix in the interlayer space. The photocatalytic activity of $H_2La_2Ti_3O_{10}{\times}BuNH_2$/Pt was found to be strongly pH-dependent, reaching maximum values in acidic medium (pH < 3) and monotonously decreasing about 10 times, while the reaction medium changed to alkaline (pH > 12). Such behavior is not typical of either the initial $H_2La_2Ti_3O_{10}$ or bulk TiO_2 and, thus, indicates a special reaction mechanism, probably involving the interlayer space as a special reaction zone.

Author Contributions: Conceptualization, I.A.R., O.I.S. and I.A.Z.; methodology, I.A.R., O.I.S. and S.A.K.; investigation, E.O.G. and A.S.M.; data curation, I.A.R. and E.O.G.; writing—original draft preparation, I.A.R. and S.A.K.; writing—review and editing, I.A.R., S.A.K., O.I.S. and I.A.Z.; visualization, I.A.R.; supervision, I.A.Z.; funding acquisition, I.A.Z. All authors have read and agreed to the published version of the manuscript.

Funding: This research was funded by the Russian Science Foundation (grant NO. 19-13-00184).

Data Availability Statement: Not applicable.

Acknowledgments: The study was technically supported by the Saint Petersburg State University Research Park. The authors are grateful to the Center for X ray Diffraction Studies, Center for Thermal Analysis and Calorimetry, Center for Chemical Analysis and Materials Research, Magnetic Resonance Research Center, Center for Diagnostics of Functional Materials for Medicine, Pharmacology and Nanoelectronics, Interdisciplinary Resource Center for Nanotechnology.

Conflicts of Interest: The authors declare no conflicts of interest.

References

1. Moiseev, I.I. Green Chemistry: Development Trajectory. *Russ. Chem. Rev.* **2013**, *82*, 616–623. https://doi.org/10.1070/rc2013v082n07abeh004393.
2. Kozlova, E.A.; Parmon, V.N. Heterogeneous Semiconductor Photocatalysts for Hydrogen Production from Aqueous Solutions of Electron Donors. *Russ. Chem. Rev.* **2017**, *86*, 870–906. https://doi.org/10.1070/rcr4739.
3. Chen, X.; Zhao, J.; Li, G.; Zhang, D.; Li, H. Recent Advances in Photocatalytic Renewable Energy Production. *Energy Mater.* **2022**, *2*, 10. https://doi.org/10.20517/energymater.2021.24.
4. Fujishima, A.; Honda, K. Electrochemical Photolysis of Water at a Semiconductor Electrode. *Nature* **1972**, *238*, 37–38. https://doi.org/10.1038/238038a0.
5. Rozhkova, E.; Ariga, K. *From Molecules to Materials Pathways to Artificial Photosynthesis*; Springer: Berlin/Heidelberg, Germany, 2015.
6. Ismail, A.A.; Bahnemann, D.W. Photochemical Splitting of Water for Hydrogen Production by Photocatalysis: A Review. *Sol. Energy Mater. Sol. Cells* ***2014***, *128*, 85–101. https://doi.org/10.1016/j.solmat.2014.04.037.
7. Ahmad, H.; Kamarudin, S.K.; Minggu, L.J.; Kassim, M. Hydrogen from Photo-Catalytic Water Splitting Process: A Review. *Renew. Sustain. Energy Rev.* **2015**, *43*, 599–610. https://doi.org/10.1016/j.rser.2014.10.101.
8. Takanabe, K. Photocatalytic Water Splitting: Quantitative Approaches toward Photocatalyst by Design. *ACS Catal.* **2017**, *7*, 8006–8022. https://doi.org/10.1021/acscatal.7b02662.
9. Walter, M.G.; Warren, E.L.; McKone, J.R.; Boettcher, S.W.; Mi, Q.; Santori, E.A.; Lewis, N.S. Solar Water Splitting Cells. *Chem. Rev.* **2010**, *110*, 6446–6473. https://doi.org/10.1021/cr1002326.
10. Kausar, F.; Varghese, A.; Pinheiro, D.; Devi, K.R.S. Recent Trends in Photocatalytic Water Splitting Using Titania Based Ternary Photocatalysts—A Review. *Int. J. Hydrog. Energy* **2022**, *47*, 22371–22402. https://doi.org/10.1016/J.IJHYDENE.2022.05.058.
11. Zhao, H.; Mao, Q.; Jian, L.; Dong, Y.; Zhu, Y. Photodeposition of Earth-Abundant Cocatalysts in Photocatalytic Water Splitting: Methods, Functions, and Mechanisms. *Chin. J. Catal.* **2022**, *43*, 1774–1804. https://doi.org/10.1016/S1872-2067(22)64105-6.
12. Moridon, S.N.F.; Arifin, K.; Yunus, R.M.; Minggu, L.J.; Kassim, M.B. Photocatalytic Water Splitting Performance of TiO_2 Sensitized by Metal Chalcogenides: A Review. *Ceram. Int.* **2022**, *48*, 5892–5907. https://doi.org/10.1016/J.CERAMINT.2021.11.199.
13. Li, R.; Li, C. Scalable Solar Water Splitting Using Particulate Photocatalysts. *Curr. Opin. Green Sustain. Chem.* **2022**, *33*, 100577. https://doi.org/10.1016/J.COGSC.2021.100577.
14. O'Neill, J.S.; Kearney, L.; Brandon, M.P.; Pryce, M.T. Design Components of Porphyrin-Based Photocatalytic Hydrogen Evolution Systems: A Review. *Coord. Chem. Rev.* **2022**, *467*, 214599. https://doi.org/10.1016/J.CCR.2022.214599.
15. Bie, C.; Wang, L.; Yu, J. Challenges for Photocatalytic Overall Water Splitting. *Chem* **2022**, *8*, 1567–1574. https://doi.org/10.1016/J.CHEMPR.2022.04.013.
16. Gupta, A.; Likozar, B.; Jana, R.; Chanu, W.C.; Singh, M.K. A Review of Hydrogen Production Processes by Photocatalytic Water Splitting—From Atomistic Catalysis Design to Optimal Reactor Engineering. *Int. J. Hydrog. Energy* **2022**, *47*, 33282–33307. https://doi.org/10.1016/J.IJHYDENE.2022.07.210.
17. Hota, P.; Das, A.; Maiti, D.K. A Short Review on Generation of Green Fuel Hydrogen through Water Splitting. *Int. J. Hydrog. Energy* **2022**, *in press*. https://doi.org/10.1016/J.IJHYDENE.2022.09.264.
18. Jiang, Z.; Ye, Z.; Shangguan, W. Recent Advances of Hydrogen Production through Particulate Semiconductor Photocatalytic Overall Water Splitting. *Front. Energy* **2022**, *16*, 49–63. https://doi.org/10.1007/s11708-022-0817-9.
19. Yao, Y.; Gao, X.; Meng, X. Recent Advances on Electrocatalytic and Photocatalytic Seawater Splitting for Hydrogen Evolution. *Int. J. Hydrog. Energy* **2021**, *46*, 9087–9100. https://doi.org/10.1016/j.ijhydene.2020.12.212.
20. Boumeriame, H.; Da Silva, E.S.; Cherevan, A.S.; Chafik, T.; Faria, J.L.; Eder, D. Layered Double Hydroxide (LDH)-Based Materials: A Mini-Review on Strategies to Improve the Performance for Photocatalytic Water Splitting. *J. Energy Chem.* **2021**, *64*, 406–431. https://doi.org/10.1016/j.jechem.2021.04.050.
21. Zhang, F.; Wang, Q. Redox-Mediated Electrocatalytic and Photocatalytic Hydrogen Production. *Curr. Opin. Electrochem.* **2022**, *35*, 101097. https://doi.org/10.1016/J.COELEC.2022.101097.
22. Sahani, S.; Malika Tripathi, K.; Il Lee, T.; Dubal, D.P.; Wong, C.P.; Chandra Sharma, Y.; Young Kim, T. Recent Advances in Photocatalytic Carbon-Based Materials for Enhanced Water Splitting under Visible-Light Irradiation. *Energy Convers. Manag.* **2022**, *252*, 115133. https://doi.org/10.1016/J.ENCONMAN.2021.115133.
23. Chen, J.; Abazari, R.; Adegoke, K.A.; Maxakato, N.W.; Bello, O.S.; Tahir, M.; Tasleem, S.; Sanati, S.; Kirillov, A.M.; Zhou, Y. Metal–Organic Frameworks and Derived Materials as Photocatalysts for Water Splitting and Carbon Dioxide Reduction. *Coord. Chem. Rev.* **2022**, *469*, 214664. https://doi.org/10.1016/J.CCR.2022.214664.

24. Jaryal, R.; Kumar, R.; Khullar, S. Mixed Metal-Metal Organic Frameworks (MM-MOFs) and Their Use as Efficient Photocatalysts for Hydrogen Evolution from Water Splitting Reactions. *Coord. Chem. Rev.* **2022**, *464*, 214542. https://doi.org/10.1016/J.CCR.2022.214542.
25. Pattanayak, P.; Singh, P.; Bansal, N.K.; Paul, M.; Dixit, H.; Porwal, S.; Mishra, S.; Singh, T. Recent Progress in Perovskite Transition Metal Oxide-Based Photocatalyst and Photoelectrode Materials for Solar-Driven Water Splitting. *J. Environ. Chem. Eng.* **2022**, *10*, 108429. https://doi.org/10.1016/J.JECE.2022.108429.
26. Liu, Y.; Yang, B.; He, H.; Yang, S.; Duan, X.; Wang, S. Bismuth-Based Complex Oxides for Photocatalytic Applications in Environmental Remediation and Water Splitting: A Review. *Sci. Total Environ.* **2022**, *804*, 150215. https://doi.org/10.1016/J.SCITOTENV.2021.150215.
27. Subramanyam, P.; Meena, B.; Biju, V.; Misawa, H.; Challapalli, S. Emerging Materials for Plasmon-Assisted Photoelectrochemical Water Splitting. *J. Photochem. Photobiol. C Photochem. Rev.* **2022**, *51*, 100472. https://doi.org/10.1016/J.JPHOTOCHEMREV.2021.100472.
28. Christoforidis, K.C.; Fornasiero, P. Photocatalytic Hydrogen Production: A Rift into the Future Energy Supply. *ChemCatChem* **2017**, *9*, 1523–1544. https://doi.org/10.1002/cctc.201601659.
29. Puga, A.V. Photocatalytic Production of Hydrogen from Biomass-Derived Feedstocks. *Coord. Chem. Rev.* **2016**, *315*, 1–66. https://doi.org/10.1016/j.ccr.2015.12.009.
30. Liu, R.; Yoshida, H.; Fujita, S. ichiro; Arai, M. Photocatalytic Hydrogen Production from Glycerol and Water with NiO_x/TiO_2 Catalysts. *Appl. Catal. B Environ.* **2014**, *144*, 47–45. https://doi.org/10.1016/j.apcatb.2013.06.024.
31. Taboada, E.; Angurell, I.; Llorca, J. Hydrogen Photoproduction from Bio-Derived Alcohols in an Optical Fiber Honeycomb Reactor Loaded with Au/TiO_2. *J. Photochem. Photobiol. A Chem.* **2014**, *281*, 35–39. https://doi.org/10.1016/j.jphotochem.2014.03.004.
32. Al-Azri, Z.H.N.; Chen, W.T.; Chan, A.; Jovic, V.; Ina, T.; Idriss, H.; Waterhouse, G.I.N. The Roles of Metal Co-Catalysts and Reaction Media in Photocatalytic Hydrogen Production: Performance Evaluation of M/TiO_2 Photocatalysts (M = Pd, Pt, Au) in Different Alcohol-Water Mixtures. *J. Catal.* **2015**, *329*, 355–367. https://doi.org/10.1016/j.jcat.2015.06.005.
33. Dosado, A.G.; Chen, W.T.; Chan, A.; Sun-Waterhouse, D.; Waterhouse, G.I.N. Novel Au/TiO_2 Photocatalysts for Hydrogen Production in Alcohol-Water Mixtures Based on Hydrogen Titanate Nanotube Precursors. *J. Catal.* **2015**, *330*, 238–254. https://doi.org/10.1016/j.jcat.2015.07.014.
34. Wang, X.; Dong, H.; Hu, Z.; Qi, Z.; Li, L. Fabrication of a $Cu_2O/Au/TiO_2$ Composite Film for Efficient Photocatalytic Hydrogen Production from Aqueous Solution of Methanol and Glucose. *Mater. Sci. Eng. B Solid State Mater. Adv. Technol.* **2017**, *219*, 10–19. https://doi.org/10.1016/j.mseb.2017.02.011.
35. Li, C.; Wang, H.; Ming, J.; Liu, M.; Fang, P. Hydrogen Generation by Photocatalytic Reforming of Glucose with Heterostructured CdS/MoS_2 Composites under Visible Light Irradiation. *Int. J. Hydrog. Energy* **2017**, *42*, 16968–16978. https://doi.org/10.1016/j.ijhydene.2017.05.137.
36. Jaswal, R.; Shende, R.; Nan, W.; Shende, A. Photocatalytic Reforming of Pinewood (Pinus Ponderosa) Acid Hydrolysate for Hydrogen Generation. *Int. J. Hydrog. Energy* **2017**, *42*, 2839–2848. https://doi.org/10.1016/j.ijhydene.2016.12.006.
37. Bellardita, M.; García-López, E.I.; Marcì, G.; Palmisano, L. Photocatalytic Formation of H_2 and Value-Added Chemicals in Aqueous Glucose (Pt)-TiO_2 Suspension. *Int. J. Hydrog. Energy* **2016**, *41*, 5934–5947. https://doi.org/10.1016/j.ijhydene.2016.02.103.
38. Zhou, M.; Li, Y.; Peng, S.; Lu, G.; Li, S. Effect of Epimerization of D-Glucose on Photocatalytic Hydrogen Generation over Pt/TiO_2. *Catal. Commun.* **2012**, *18*, 21–25. https://doi.org/10.1016/j.catcom.2011.11.017.
39. Bahadori, E.; Ramis, G.; Zanardo, D.; Menegazzo, F.; Signoretto, M.; Gazzoli, D.; Pietrogiacomi, D.; Di Michele, A. Photoreforming of Glucose over CuO/TiO_2. *Catalysts* **2020**, *10*, 477. https://doi.org/10.3390/catal10050477.
40. Bellardita, M.; García-López, E.I.; Marcì, G.; Nasillo, G.; Palmisano, L. Photocatalytic Solar Light H_2 Production by Aqueous Glucose Reforming. *Eur. J. Inorg. Chem.* **2018**, *2018*, 4522–4532. https://doi.org/10.1002/ejic.201800663.
41. Iervolino, G.; Vaiano, V.; Murcia, J.J.; Rizzo, L.; Ventre, G.; Pepe, G.; Campiglia, P.; Hidalgo, M.C.; Navío, J.A.; Sannino, D. Photocatalytic Hydrogen Production from Degradation of Glucose over Fluorinated and Platinized TiO_2 Catalysts. *J. Catal.* **2016**, *339*, 47–56. https://doi.org/10.1016/j.jcat.2016.03.032.
42. Zhao, H.; Li, C.F.; Yong, X.; Kumar, P.; Palma, B.; Hu, Z.Y.; Van Tendeloo, G.; Siahrostami, S.; Larter, S.; Zheng, D.; et al. Coproduction of Hydrogen and Lactic Acid from Glucose Photocatalysis on Band-Engineered $Zn_{1-x}Cd_xS$ Homojunction. *iScience* **2021**, *24*, 102109. https://doi.org/10.1016/j.isci.2021.102109.
43. Zheng, X.; Wang, X.; Liu, J.; Fu, X.; Yang, Y.; Han, H.; Fan, Y.; Zhang, S.; Meng, S.; Chen, S. Construction of $NiP_x/MoS_2/NiS/CdS$ Composite to Promote Photocatalytic H2 Production from Glucose Solution. *J. Am. Ceram. Soc.* **2021**, *104*, 5307–5316. https://doi.org/10.1111/jace.17883.
44. Speltini, A.; Scalabrini, A.; Maraschi, F.; Sturini, M.; Pisanu, A.; Malavasi, L.; Profumo, A. Improved Photocatalytic H_2 Production Assisted by Aqueous Glucose Biomass by Oxidized g-C_3N_4. *Int. J. Hydrog. Energy* **2018**, *43*, 14925–14933. https://doi.org/10.1016/j.ijhydene.2018.06.103.
45. Bai, X.; Hou, Q.; Qian, H.; Nie, Y.; Xia, T.; Lai, R.; Yu, G.; Laiq Ur Rehman, M.; Xie, H.; Ju, M. Selective Oxidation of Glucose to Gluconic Acid and Glucaric Acid with Chlorin E6 Modified Carbon Nitride as Metal-Free Photocatalyst. *Appl. Catal. B Environ.* **2022**, *303*, 120895. https://doi.org/10.1016/j.apcatb.2021.120895.
46. Speltini, A.; Romani, L.; Dondi, D.; Malavasi, L.; Profumo, A. Carbon Nitride-Perovskite Composites: Evaluation and Optimization of Photocatalytic Hydrogen Evolution in Saccharides Aqueous Solution. *Catalysts* **2020**, *10*, 1259. https://doi.org/10.3390/catal10111259.

47. Rodionov, I.A.; Zvereva, I.A. Photocatalytic Activity of Layered Perovskite-like Oxides in Practically Valuable Chemical Reactions. *Russ. Chem. Rev.* **2016**, *85*, 248–279. https://doi.org/10.1070/rcr4547.
48. Schaak, R.E.; Mallouk, T.E. Perovskites by Design: A Toolbox of Solid-State Reactions. *Chem. Mater.* **2002**, *14*, 1455–1471. https://doi.org/10.1021/cm010689m.
49. Uppuluri, R.; Sen Gupta, A.; Rosas, A.S.; Mallouk, T.E. Soft Chemistry of Ion-Exchangeable Layered Metal Oxides. *Chem. Soc. Rev.* **2018**, *47*, 2401–2430. https://doi.org/10.1039/c7cs00290d.
50. Tani, S.; Komori, Y.; Hayashi, S.; Sugahara, Y. Local Environments and Dynamics of Hydrogen Atoms in Protonated Forms of Ion-Exchangeable Layered Perovskites Estimated by Solid-State ^{1}H NMR. *J. Solid State Chem.* **2006**, *179*, 3357–3364. https://doi.org/10.1016/j.jssc.2006.06.030.
51. Ladasiu, C.; Kulischow, N.; Marschall, R. Tuning the Photocatalytic Activity of Layered Perovskite Niobates by Controlled Ion Exchange and Hydration. *Catal. Sci. Technol.* **2022**, *12*, 1450–1457. https://doi.org/10.1039/d1cy02057a.
52. Liton, M.N.H.; Roknuzzaman, M.; Helal, M.A.; Kamruzzaman, M.; Islam, A.K.M.F.U.; Ostrikov, K.; Khan, M.K.R. Electronic, Mechanical, Optical and Photocatalytic Properties of Perovskite $RbSr_2Nb_3O_{10}$ Compound. *J. Alloy. Compd.* **2021**, *867*, 159077. https://doi.org/10.1016/j.jallcom.2021.159077.
53. Zou, Z.; Ye, J.; Arakawa, H. Substitution Effects of In^{3+} by Fe^{3+} on Photocatalytic and Structural Properties of Bi_2InNbO_7 Photocatalysts. *J. Mol. Catal.* **2001**, *168*, 289–297.
54. Reddy, V.; Hwang, D.; Lee, J. Effect of Zr Substitution for Ti in $KLaTiO_4$ for Photocatalytic Water Splitting. *Catal. Lett.* **2003**, *90*, 39–44, doi:1011-372X/03/0900–0039/0.
55. Kumar, V.; Govind; Uma, S. Investigation of Cation (Sn^{2+}) and Anion (N^{3-}) Substitution in Favor of Visible Light Photocatalytic Activity in the Layered Perovskite $K_2La_2Ti_3O_{10}$. *J. Hazard. Mater.* **2011**, *189*, 502–508. https://doi.org/10.1016/j.jhazmat.2011.02.064.
56. Zhou, Y.; Wen, T.; Guo, Y.; Yang, B.; Wang, Y. Controllable Doping of Nitrogen and Tetravalent Niobium Affords Yellow and Black Calcium Niobate Nanosheets for Enhanced Photocatalytic Hydrogen Evolution. *RSC Adv.* **2016**, *6*, 64930–64936. https://doi.org/10.1039/C6RA11407E.
57. Kawashima, K.; Hojamberdiev, M.; Chen, S.; Yubuta, K.; Wagata, H.; Domen, K.; Teshima, K. Understanding the Effect of Partial N^{3-}-to-O^{2-} Substitution and H^{+}-to-K^{+} Exchange on Photocatalytic Water Reduction Activity of Ruddlesden–Popper Layered Perovskite $KLaTiO_4$. *Mol. Catal.* **2017**, *432*, 250–258. https://doi.org/10.1016/j.mcat.2017.01.004.
58. Hu, Y.; Shi, J.; Guo, L. Enhanced Photocatalytic Hydrogen Production Activity of Chromium Doped Lead Niobate under Visible-Light Irradiation. *Appl. Catal. A Gen.* **2013**, *468*, 403–409. https://doi.org/10.1016/j.apcata.2013.09.015.
59. Huang, Y.; Li, J.; Wei, Y.; Li, Y.; Lin, J.; Wu, J. Fabrication and Photocatalytic Property of Pt-Intercalated Layered Perovskite Niobates $H_{1-x}LaNb_{2-x}Mo_xO_7$ (X = 0–0.15). *J. Hazard. Mater.* **2009**, *166*, 103–108. https://doi.org/10.1016/j.jhazmat.2008.11.040.
60. Huang, Y.; Li, Y.; Wei, Y.; Huang, M.; Wu, J. Photocatalytic Property of Partially Substituted Pt-Intercalated Layered Perovskite, $ASr_2Ta_xNb_{3-x}O_{10}$ (A = K, H; X = 0, 1, 1.5, 2 and 3). *Sol. Energy Mater. Sol. Cells* **2011**, *95*, 1019–1027. https://doi.org/10.1016/j.solmat.2010.12.017.
61. Oshima, T.; Wang, Y.; Lu, D.; Yokoi, T.; Maeda, K. Photocatalytic Overall Water Splitting on Pt Nanocluster-Intercalated, Restacked $KCa_2Nb_3O_{10}$ Nanosheets: The Promotional Effect of Co-Existing Ions. *Nanoscale Adv.* **2019**, *1*, 189–194. https://doi.org/10.1039/c8na00240a.
62. Cui, W.; Qi, Y.; Liu, L.; Rana, D.; Hu, J.; Liang, Y. Synthesis of PbS–$K_2La_2Ti_3O_{10}$ Composite and Its Photocatalytic Activity for Hydrogen Production. *Prog. Nat. Sci. Mater. Int.* **2012**, *22*, 120–125. https://doi.org/10.1016/j.pnsc.2012.03.002.
63. Cui, W.; Guo, D.; Liu, L.; Hu, J.; Rana, D.; Liang, Y. Preparation of $ZnIn_2S_4$/$K_2La_2Ti_3O_{10}$ Composites and Their Photocatalytic H_2 Evolution from Aqueous Na_2S/Na_2SO_3 under Visible Light Irradiation. *Catal. Commun.* **2014**, *48*, 55–59. https://doi.org/10.1016/j.catcom.2014.01.026.
64. Saito, K.; Kozeni, M.; Sohmiya, M.; Komaguchi, K.; Ogawa, M.; Sugahara, Y.; Ide, Y. Unprecedentedly Enhanced Solar Photocatalytic Activity of a Layered Titanate Simply Integrated with TiO_2 Nanoparticles. *Phys. Chem. Chem. Phys.* **2016**, *18*, 30920–30925. https://doi.org/10.1039/c6cp05635k.
65. Liu, Y.; Zhou, Y.; Lv, C.; Zhang, C.; Jin, X.; Meng, Q.; Chen, G. Construction of 2D-Composite $HCa_2Nb_3O_{10}$/$CaNb_2O_6$ Heterostructured Photocatalysts with Enhanced Hydrogen Production Performance. *New J. Chem.* **2018**, *42*, 681–687. https://doi.org/10.1039/C7NJ03707D.
66. Zheng, B.; Mao, L.; Shi, J.; Chen, Q.; Hu, Y.; Zhang, G.; Yao, J.; Lu, Y. Facile Layer-by-Layer Self-Assembly of 2D Perovskite Niobate and Layered Double Hydroxide Nanosheets for Enhanced Photocatalytic Oxygen Generation. *Int. J. Hydrog. Energy* **2021**, *46*, 34276–34286. https://doi.org/10.1016/j.ijhydene.2021.07.233.
67. Youngblood, W.J.; Anna Lee, S.H.; Maeda, K.; Mallouk, T.E. Visible Light Water Splitting Using Dye-Sensitized Oxide Semiconductors. *Acc. Chem. Res.* **2009**, *42*, 1966–1973. https://doi.org/10.1021/ar9002398.
68. Tang, L.; Zhang, Y.; Foo, M.L.; Xu, Q.; Wang, P.; Xu, C.; Wang, J.; Chen, W.Q. Preparation of CdS/$Cs_{0.68}Ti_{1.83}O_4$ Heterojunction for Promoted Photocatalytic Hydrogen Evolution Reaction. *J. Alloys Compd.* **2021**, *876*, 160097. https://doi.org/10.1016/j.jallcom.2021.160097.
69. Hu, Y.; Mao, L.; Guan, X.; Tucker, K.A.; Xie, H.; Wu, X.; Shi, J. Layered Perovskite Oxides and Their Derivative Nanosheets Adopting Different Modification Strategies towards Better Photocatalytic Performance of Water Splitting. *Renew. Sustain. Energy Rev.* **2020**, *119*, 109527. https://doi.org/10.1016/j.rser.2019.109527.

70. Chang, C.W.; Nurpratiwi, A.A.; Su, Y.H. A Comparison Study of Molten-Salt and Solid-State Method for the Photoelectrochemical Water Splitting Performance of Dion-Jacobson Layers Perovskite $Ca_2Na_{n-3}Nb_nO_{3n+1}$- (n = 4, 5, and 6) Nanosheets. *Int. J. Hydrog. Energy* **2022**, *47*, 40573–40581. https://doi.org/10.1016/j.ijhydene.2021.07.227.
71. Rodionov, I.A.; Silyukov, O.I.; Utkina, T.D.; Chislov, M.V.; Sokolova, Y.P.; Zvereva, I.A. Photocatalytic Properties and Hydration of Perovskite-Type Layered Titanates $A_2Ln_2Ti_3O_{10}$ (A = Li, Na, K; Ln = La, Nd). *Russ. J. Gen. Chem.* **2012**, *82*, 1191–1196. https://doi.org/10.1134/S1070363212070018.
72. Takata, T.; Furumi, Y.; Shinohara, K.; Tanaka, A.; Hara, M.; Kondo, J.N.; Domen, K. Photocatalytic Decomposition of Water on Spontaneously Hydrated Layered Perovskites. *Chem. Mater.* **1997**, *9*, 1063–1064. https://doi.org/10.1021/cm960612b.
73. Cui, W.; Liu, L.; Ma, S.; Liang, Y.; Zhang, Z. CdS-Sensitized $K_2La_2Ti_3O_{10}$ Composite: A New Photocatalyst for Hydrogen Evolution under Visible Light Irradiation. *Catal. Today* **2013**, *207*, 44–49. https://doi.org/10.1016/j.cattod.2012.05.009.
74. Constantino, V.R.L.; Barbosa, C.A.S.; Bizeto, M.A.; Dias, P.M. Intercalation Compounds Involving Inorganic Layered Structures. *An. Acad. Bras. Cienc.* **2000**, *72*, 45–50. https://doi.org/10.1590/S0001-37652000000100006.
75. Jacobson, A.J.; Johnson, J.W.; Lewandowski, J. Intercalation of the Layered Solid Acid $HCa_2Nb_3O_{10}$ by Organic Amines. *Mater. Res. Bull.* **1987**, *22*, 45–51. https://doi.org/10.1016/0025-5408(87)90148-6.
76. Minich, I.A.; Silyukov, O.I.; Kurnosenko, S.A.; Gak, V.V.; Kalganov, V.D.; Kolonitskiy, P.D.; Zvereva, I.A. Physical–Chemical Exfoliation of *n*-Alkylamine Derivatives of Layered Perovskite-like Oxide $H_2K_{0.5}Bi_{2.5}Ti_4O_{13}$ into Nanosheets. *Nanomaterials* **2021**, *11*, 2708. https://doi.org/10.3390/nano11102708.
77. Tahara, S.; Sugahara, Y. Interlayer Surface Modification of the Protonated Triple-Layered Perovskite $HCa_2Nb_3O_{10}{\cdot}xH_2O$ with *n*-Alcohols. *Langmuir* **2003**, *19*, 9473–9478. https://doi.org/10.1021/la0343876.
78. Tahara, S.; Ichikawa, T.; Kajiwara, G.; Sugahara, Y. Reactivity of the Ruddlesden−Popper Phase $H_2La_2Ti_3O_{10}$ with Organic Compounds: Intercalation and Grafting Reactions. *Chem. Mater.* **2007**, *19*, 2352–2358. https://doi.org/10.1021/cm0623662.
79. Kurnosenko, S.A.; Voytovich, V.V.; Silyukov, O.I.; Minich, I.A.; Malygina, E.N.; Zvereva, I.A. Inorganic-Organic Derivatives of Layered Perovskite-like Titanates $HLnTiO_4$ (Ln = La, Nd) with *n*-Amines and *n*-Alcohols: Synthesis, Thermal, Vacuum and Hydrolytic Stability. *Ceram. Int.* **2022**, *48*, 7240–7252. https://doi.org/10.1016/j.ceramint.2021.11.284.
80. Wang, C.; Tang, K.; Wang, D.; Liu, Z.; Wang, L.; Zhu, Y.; Qian, Y. A New Carbon Intercalated Compound of Dion–Jacobson Phase $HLaNb_2O_7$. *J. Mater. Chem.* **2012**, *22*, 11086. https://doi.org/10.1039/c2jm14902h.
81. Aznar, A.J.; Sanz, J.; Ruiz-Hitzky, E. Mechanism of the Grafting of Organosilanes on Mineral Surfaces. IV. Phenylderivatives of Sepiolite and Poly (Organosiloxanes). *Colloid Polym. Sci.* **1992**, *270*, 165–176. https://doi.org/10.1007/BF00652183.
82. Shimada, A.; Yoneyama, Y.; Tahara, S.; Mutin, P.H.; Sugahara, Y. Interlayer Surface Modification of the Protonated Ion-Exchangeable Layered Perovskite $HLaNb_2O_7{\times}H_2O$ with Organophosphonic Acids. *Chem. Mater.* **2009**, *21*, 4155–4162. https://doi.org/10.1021/cm900228c.
83. Sanchez, C.; Gomez-Romero, P. *Functional Hybrid Materials*; Wiley-VCH Verlag GmbH & Co. KGaA: Weinheim, Germany, 2006; ISBN 3527303596.
84. Kickelbick, G. *Hybrid Materials: Synthesis, Characterization, and Applications*; Wiley-VCH Verlag GmbH & Co. KGaA: Weinheim, Germany, 2007; ISBN 9783527312993.
85. Mir, S.H.; Nagahara, L.A.; Thundat, T.; Mokarian-Tabari, P.; Furukawa, H.; Khosla, A. Review—Organic-Inorganic Hybrid Functional Materials: An Integrated Platform for Applied Technologies. *J. Electrochem. Soc.* **2018**, *165*, B3137–B3156. https://doi.org/10.1149/2.0191808jes.
86. Machida, M.; Mitsuyama, T.; Ikeue, K.; Matsushima, S.; Arai, M. Photocatalytic Property and Electronic Structure of Triple-Layered Perovskite Tantalates, $MCa_2Ta_3O_{10}$ (M = Cs, Na, H, and $C_6H_{13}NH_3$). *J. Phys. Chem. B* **2005**, *109*, 7801–7806. https://doi.org/10.1021/jp044833d.
87. Wang, Y.; Wang, C.; Wang, L.; Hao, Q.; Zhu, X.; Chen, X.; Tang, K. Preparation of Interlayer Surface Tailored Protonated Double-Layered Perovskite $H_2CaTa_2O_7$ with *n*-Alcohols, and Their Photocatalytic Activity. *RSC Adv.* **2014**, *4*, 4047–4054. https://doi.org/10.1039/C3RA44623A.
88. Guo, T.; Wang, L.; Evans, D.G.; Yang, W. Synthesis and Photocatalytic Properties of a Polyaniline-Intercalated Layered Protonic Titanate Nanocomposite with a p−n Heterojunction Structure. *J. Phys. Chem. C* **2010**, *114*, 4765–4772. https://doi.org/10.1021/jp9055413.
89. Liu, C.; Wu, L.; Chen, J.; Liang, J.Y.; Li, C.S.; Ji, H.M.; Hou, W.H. The Nanocomposite of Polyaniline and Nitrogen-Doped Layered $HTiNbO_5$ with Excellent Visible-Light Photocatalytic Performance. *Phys. Chem. Chem. Phys.* **2014**, *16*, 13409–13417. https://doi.org/10.1039/c4cp01423e.
90. Zhu, H.; Yao, X.; Hua, S. Nanocomposite of Polyaniline and a Layered Niobate Acid Host: Synthesis, Electrochemical Studies, and Photocatalytic Properties. *Polym. Compos.* **2013**, *34*, 834–841. https://doi.org/10.1002/pc.22485.
91. Rodionov, I.A.; Maksimova, E.A.; Pozhidaev, A.Y.; Kurnosenko, S.A.; Silyukov, O.I.; Zvereva, I.A. Layered Titanate $H_2Nd_2Ti_3O_{10}$ Intercalated With *n*-Butylamine: A New Highly Efficient Hybrid Photocatalyst for Hydrogen Production From Aqueous Solutions of Alcohols. *Front. Chem.* **2019**, *7*, 863. https://doi.org/10.3389/fchem.2019.00863.
92. Voytovich, V.V.; Kurnosenko, S.A.; Silyukov, O.I.; Rodionov, I.A.; Minich, I.A.; Zvereva, I.A. Study of N-Alkylamine Intercalated Layered Perovskite-Like Niobates $HCa_2Nb_3O_{10}$ as Photocatalysts for Hydrogen Production From an Aqueous Solution of Methanol. *Front. Chem.* **2020**, *8*, 300. https://doi.org/10.3389/fchem.2020.00300.
93. Voytovich, V.V.; Kurnosenko, S.A.; Silyukov, O.I.; Rodionov, I.A.; Bugrov, A.N.; Minich, I.A.; Malygina, E.N.; Zvereva, I.A. Synthesis of *n*-Alkoxy Derivatives of Layered Perovskite-Like Niobate $HCa_2Nb_3O_{10}$ and Study of Their Photocatalytic Activity for Hydrogen Production from an Aqueous Solution of Methanol. *Catalysts* **2021**, *11*, 897. https://doi.org/10.3390/catal11080897.

94. Kurnosenko, S.A.; Voytovich, V.V.; Silyukov, O.I.; Rodionov, I.A.; Kirichenko, S.O.; Minich, I.A.; Malygina, E.N.; Khramova, A.D.; Zvereva, I.A. Photocatalytic Activity of *n*-Alkylamine and *n*-Alkoxy Derivatives of Layered Perovskite-like Titanates $H_2Ln_2Ti_3O_{10}$ (Ln = La, Nd) in the Reaction of Hydrogen Production from an Aqueous Solution of Methanol. *Catalysts* **2021**, *11*, 1279. https://doi.org/10.3390/catal11111279.
95. Kurnosenko, S.A.; Voytovich, V.V.; Silyukov, O.I.; Rodionov, I.A.; Zvereva, I.A. Photocatalytic Hydrogen Production from Aqueous Solutions of Glucose and Xylose over Layered Perovskite-like Oxides $HCa_2Nb_3O_{10}$, $H_2La_2Ti_3O_{10}$ and Their Inorganic-Organic Derivatives. *Nanomaterials* **2022**, *12*, 2717. https://doi.org/10.3390/nano12152717.
96. Rodionov, I.A.; Mechtaeva, E.V.; Burovikhina, A.A.; Silyukov, O.I.; Toikka, M.A.; Zvereva, I.A. Effect of Protonation on the Photocatalytic Activity of the $K_2La_2Ti_3O_{10}$ Layered Oxide in the Reaction of Hydrogen Production. *Mon. Chem. Chem. Mon.* **2018**, *149*, 475–482. https://doi.org/10.1007/s00706-017-2105-7.
97. Silyukov, O.; Chislov, M.; Burovikhina, A.; Utkina, T.; Zvereva, I. Thermogravimetry Study of Ion Exchange and Hydration in Layered Oxide Materials. *J. Therm. Anal. Calorim.* **2012**, *110*, 187–192. https://doi.org/10.1007/s10973-012-2198-5.
98. Li, Z.; Ivanenko, A.; Meng, X.; Zhang, Z. Photocatalytic Oxidation of Methanol to Formaldehyde on Bismuth-Based Semiconductors. *J. Hazard. Mater.* **2019**, *380*, 120822. https://doi.org/10.1016/j.jhazmat.2019.120822.
99. Panayotov, D.A.; Burrows, S.P.; Morris, J.R. Photooxidation Mechanism of Methanol on Rutile TiO_2 Nanoparticles. *J. Phys. Chem. C* **2012**, *116*, 6623–6635. https://doi.org/10.1021/jp209215c.
100. Kolesov, G.; Vinichenko, D.; Tritsaris, G.A.; Friend, C.M.; Kaxiras, E. Anatomy of the Photochemical Reaction: Excited-State Dynamics Reveals the C-H Acidity Mechanism of Methoxy Photo-Oxidation on Titania. *J. Phys. Chem. Lett.* **2015**, *6*, 1624–1627. https://doi.org/10.1021/acs.jpclett.5b00429.
101. Karimi Estahbanati, M.R.; Mahinpey, N.; Feilizadeh, M.; Attar, F.; Iliuta, M.C. Kinetic Study of the Effects of pH on the Photocatalytic Hydrogen Production from Alcohols. *Int. J. Hydrog. Energy* **2019**, *44*, 32030–32041. https://doi.org/10.1016/j.ijhydene.2019.10.114.
102. Rodionov, I.A.; Sokolova, I.P.; Silyukov, O.I.; Burovikhina, A.A.; Fateev, S.A.; Zvereva, I.A. Protonation and Photocatalytic Activity of the $Rb_2La_2Ti_3O_{10}$ Layered Oxide in the Reaction of Hydrogen Production. *Int. J. Photoenergy* **2017**, *2017*, 9628146. https://doi.org/10.1155/2017/9628146.
103. Rodionov, I.A.; Fateev, S.A.; Zvereva, I.A. Effect of Protonation on the Photocatalytic Activity of the Layered Titanate $Rb_2Nd_2Ti_3O_{10}$. *Russ. J. Gen. Chem.* **2017**, *87*, 2728–2729. https://doi.org/10.1134/S1070363217110317.